Characteristic Energies and Shifts in Optical Spectra of Colloidal IV−VI Semiconductor Nanocrystals

R. Leitsmann[†,‡,*] and F. Bechstedt[†]

[†]European Theoretical Spectroscopy Facility (ETSF) and Institut für Festkörpertheorie und -optik, Friedrich-Schiller-Universität Jena, Max-Wien-Platz 1, 07743 Jena, Germany, and [‡]GWT-TUD GmbH, Material Calculations, Annabergerstr. 240, 09125 Chemnitz, Germany

ABSTRACT We investigate structural, electronic, and optical properties of colloidal IV−VI semiconductor quantum dots (QDs) using an *ab initio* pseudopotential method and a repeated supercell approximation. In particular, rhombo-cuboctahedral quantum dots consisting of PbSe, PbTe, and SnTe with a pseudohydrogen passivation shell are investigated for different QD sizes. The obtained dependence of the confinement energy on the QD size questions the use of three-dimensional spherical potential well models for small QD structures. The predicted band gaps are almost in agreement with measured values. The calculated Franck−Condon shifts vary significantly with the QD size. Only for PbSe they may explain the Stokes shift between optical absorption and emission. For the tellurides, spectral properties such as the oscillator strength are more important.

KEYWORDS: *ab initio* · nanocrystals · lead salts · photoluminescence · confinement energy

The efficient multiple-exciton generation discovered in lead chalcogenide nanocrystals (NCs)[1−3] opens the possibility of generating several electron−hole pairs from a single, high-energy photon. This mechanism potentially increases the optical efficiency of these nanosystems and makes them promising candidates for light sources in the mid-infrared spectral region or for light absorbers in third-generation solar-cell devices. Recent progress has been made in synthesizing colloidal NCs made of narrow-gap semiconductors such as PbS, PbSe, and PbTe.[4−6] Typically, the band gaps of these materials can be tuned between 0.5 and 1.5 eV, which covers the entire near-infrared spectral region. On the other hand, the synthesis of NCs with band gaps smaller than 0.5 eV is still a challenging task.[7]

The theoretical *ab initio* description of IV−VI materials is also ambitious for different reasons. There is a remarkable ionic contribution to the chemical bonding. As a consequence, most of the common IV−VI semiconductors crystallize in rocksalt (rs) structure with the space group $Fm3m$ (O_h^5). In addition, PbTe and SnTe exhibit shallow cation-derived d states.[8] Therefore, one has to treat (beside the s,p states) the outermost d electrons of the group IV elements as valence electrons. On the other hand, for a precise description of heavy elements like Pb, the inclusion of relativistic effects (*e.g.*, spin−orbit coupling, SOC) is necessary.[9,10] One question, which arises, is whether the replacement of Pb with the lighter atom Sn may reduce these effects. Furthermore, to be able to compare theoretical results to experimental findings for realistic NC sizes, one has to use huge supercells. This increases the computational cost of the calculations considerably.

In the present article, we focus on the description of rhombo-cuboctahedral IV−VI semiconductor quantum dots (QDs) with a pseudohydrogen passivation shell. Pseudohydrogen atoms with 1/3 (H) or 5/3 (H*) electrons are used.[8,11] In the center of these structures can be either an anion or a cation, which leads to different surface terminations due to the shellwise construction. The differently sized NCs are denoted as QD-*da* and QD-*dc*, were *d* is the diameter in units of the bulk lattice constant a_0 and *a*/*c* describe the ionic character (anion/cation) of the central atom.

RESULTS AND DISCUSSION

Structural Properties. Independent of the character of the central ion, the structural optimization of the IV−VI semiconductor quantum dots almost conserves the six-fold coordinated rs structure of the bulk phase of these compounds. This is illustrated in Figure 1, where we show the optimized structure of 0.64 nm (QD-1a), 1.28 nm (QD-2a), and 1.92 nm

*Address correspondence to roman@ifto.physik.uni-jena.de.

Received for review August 11, 2009 and accepted October 23, 2009.

Published online October 29, 2009.
10.1021/nn900987j CCC: $40.75

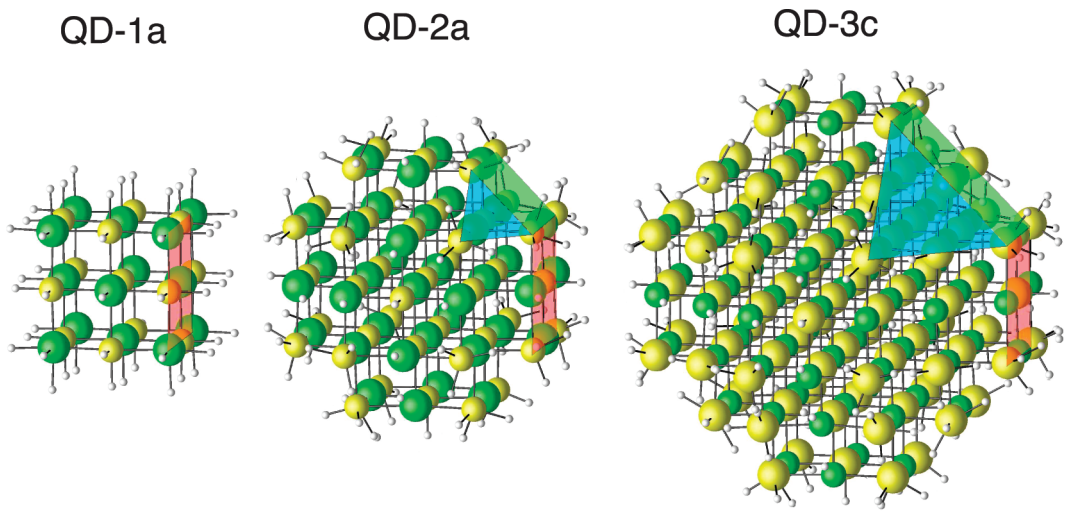

Figure 1. Optimized bonding geometry of three differently sized IV−VI quantum dots. The green, yellow, and white balls represent cations, anions, and pseudohydrogen atoms, respectively.

(QD-3c) PbTe QDs, or more precisely $Pb_{14}Te_{13}H_{24}H^*_{30}$, $Pb_{38}Te_{43}H_{78}H^*_{48}$, and $Pb_{79}Te_{92}H_{150}H^*_{72}$ clusters. Even at the surface facets, the rs structure remains stable. Therefore, the original O_h point symmetry of the bulk phase is kept. The occurring surface facets are indicated in Figure 1 by red (100), green (110), and blue (111) planes. While the (100) and (110) planes contain the same number of anions and cations, the (111) planes lead to differently anion- or cation-terminated surfaces. However, due to the occurring O_h symmetry, the appearance of surface-induced macroscopic electrostatic fields is suppressed. For a quantitative analysis of the QD structure, the IV−VI bond lengths are a good measure. Although the largest bond length deviations close to the NC surface can reach values up to 6% of the bulk equilibrium bond length, the average IV−VI bond length deviations remain small (Figure 2). Compared to the bulk bond length, we obtain a small reduction, which increases with decreasing NC diameter, D_{NC}, in good agreement with other theoretical results obtained for PbSe QDs.[12] This behavior may be modeled *via*

$$d^{NC}_{IV-VI}[Å] = d^{bulk}_{IV-VI}[Å] - \frac{\gamma}{D^{\delta}_{NC}[Å]} \qquad (1)$$

where we determined the parameter γ to 0.08 (PbTe), 0.12 (SnTe), and 0.34 (PbSe) and the exponent δ to be 0.72 (PbTe), 0.99 (SnTe), and 0.62 (PbSe). Since γ can be interpreted as a measure for the strength of the lattice deviations, the largest differences from the ideal rocksalt structure are obtained in PbSe NCs. This is a consequence of the stronger ionic character of PbSe ($f_i = 0.76$) compared to PbTe ($f_i = 0.65$) and SnTe ($f_i = 0.63$) on the Phillips scale.[13,14] The larger electrostatic forces between the anions and cations in PbSe lead to larger adjustments of the lattice structure at the NC surfaces and hence to a larger bond length deviation. Nevertheless, the obtained bond length deviations in PbSe QDs are smaller than the results of ref 12. This is traced back to the pseudohydrogen passivation shell in our study. In general, the reduction of the IV−VI bond lengths corresponds to a compression of the nanostructured material, which becomes larger with increasing influence of the surface tension. The predicted almost conservation of the ideal rs structure is in agreement with recent high-resolution cross-sectional transmission electron microscopy (HRXTEM) investigations on PbSe, SnTe, and HgTe QDs.[7,15] However, the predicted behavior is in contrast to the results of the simple ionic model proposed by Perebeinos *et al.* for NCs.[16] We, thus, agree with Franceschetti[12] that such a simple ionic model is unable to describe the structural properties of IV−VI

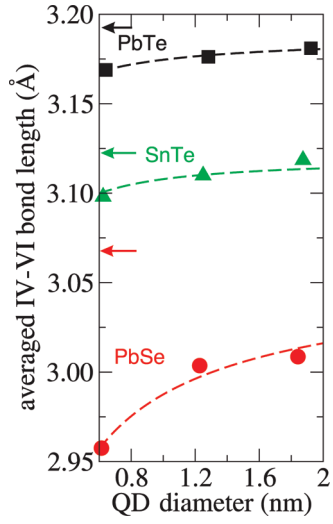

Figure 2. IV−VI bond lengths calculated for different NC diameters and materials. The filled symbols represent average bond lengths. Squares (black), triangles (green), and circles (red) represent PbTe, SnTe, and PbSe, respectively. The theoretical bulk bond lengths are indicated by arrows. Dashed lines are fits using eq 1.

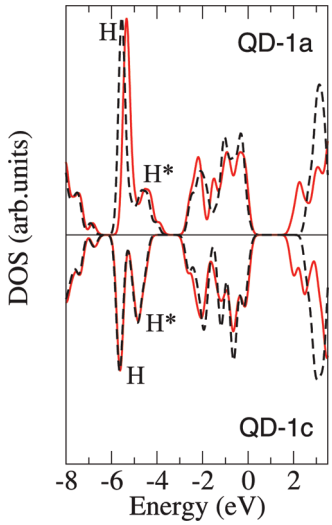

Figure 3. Density of states of the smallest PbTe NC with a central anion (QD-1a, upper panel) or a central cation (QD-1c, lower panel). The black dashed line corresponds to Kohn−Sham energies within DFT-LDA and the red solid line to the inclusion of spin−orbit interaction. The passivation induced states are indicated by H and H*.

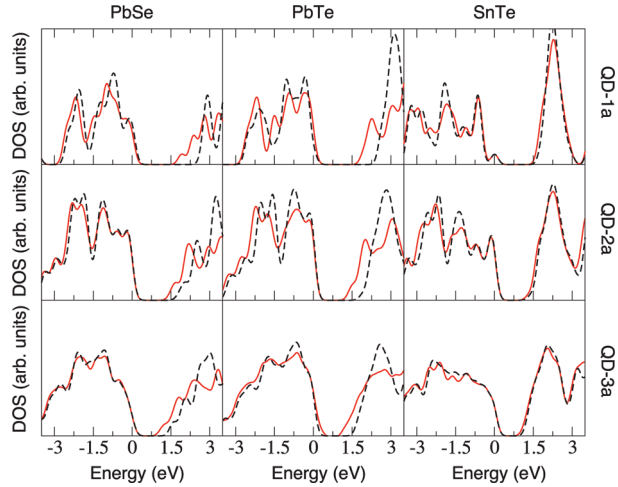

Figure 4. Density of states of IV−VI NCs without SOC (dashed black line) and with SOC (red solid line). The HONO eigenvalue is used as energy zero.

NCs accurately. In fact, surface effects play an important role.

Electronic Properties. Since the geometric properties depend only slightly on the ionic character of the central ion, we expect the same for the electronic properties. This is indeed the case as can be seen in Figure 3. The plotted density of states (DOS) for 0.62 nm PbTe QDs with either central anion (QD-1a) or cation (QD-1c) are quite similar. This holds for both treatments, with and without SOC effects. The remaining small differences around −5 eV can be traced back to the different amount of anions and cations and the resulting different surface terminations. Therefore, in the discussion below, we will concentrate on NCs with a central anion.

Due to the applied surface passivation scheme, we have saturated all dangling bonds at the QD surface. The resulting electronic states related to the surface passivation (H and H*) are well-separated from the band gap region. Hence, there influence on the electronic states close to the band edges can be neglected. In particular, the optical spectra at low frequencies will not be influenced by the passivation states. Of course, other passivation schemes with remaining dangling bonds and/or surface reconstructions will lead to different electronic and optical properties. However, the detailed discussion of those effects is beyond the aim of this study.

As can be seen in Figure 4, all investigated compounds PbTe, PbSe, and SnTe give rise to quite similar electronic properties of the NCs. The material influences mainly the size of the band gap, E_g, resulting in the general sequence $E_g(\text{PbSe}) > E_g(\text{PbTe}) > E_g(\text{SnTe})$ for all QD diameters. This series is consistent with the expectations according to the ionicities $f_i(\text{PbSe}) > f_i(\text{PbTe}) > f_i(\text{SnTe})$ (see Table 1). The material with the strongest ionic character (PbSe) shows the largest band gap because, in this case, the electrons are more strongly localized at the atomic cores. With increasing quantum dot size, the differences, however, decrease until for $D_{NC} \rightarrow \infty$ the bulk limit is reached. In this case, the chemical trend due to the ionicity is superimposed by relativistic effects. Taking into account SOC, in the bulk limit, a slightly changed band gap series appears (bulk band gaps in LSDA+SOC can be calculated as 0.21 eV (PbSe), 0.13 eV (PbTe), and 0.35 eV (SnTe)). This fact is caused by difficulties describing the band characters close to the fundamental band gap in lead salt bulk materials including SOC.[17] However, the gaps are small: of the order of a few tenths of electronvolts. In the QD systems under investigation with much larger gaps, this problem can be ignored. Due to the strong confinement effect, the highest occupied nanocrystal orbital (HONO) and the lowest unoccupied nanocrystal orbital (LUNO) are energetically well-separated. Hence, the character of the near gap states is correctly described with and without SOC.

In Figure 4, we observe a large influence of the SOC in PbSe and PbTe, while in SnTe QDs, this effect can be neglected. In PbSe and PbTe 1a-QDs, for example, the inclusion of SOC leads to a shrinkage of the LDA band gap of 0.9 and 0.7 eV, respectively. Such a band gap reduction by going over from LDA to LSDA−SOC is well-known for lead salt bulk materials. The topmost valence band is shifted upward, whereas the lowest conduction band is moved downward in energy, resulting in a

TABLE 1. Calculated Ground-State KS HONO−LUNO Band Gaps E_g with and without the Inclusion of Spin−Orbit Effects (in eV)

	PbSe			PbTe			SnTe		
D_{NC} (nm)	0.61	1.23	1.84	0.64	1.28	1.92	0.62	1.25	1.87
LSDA+SOC	1.9	1.5	1.2	1.9	1.4	1.1	1.7	1.4	1.2
LDA	2.8	1.8	1.6	2.6	1.8	1.7	1.8	1.4	1.3

significant reduction of the direct energy gap.[10,17] The reason for the much smaller SOC effect in SnTe QDs is related to the atomic weight of the cations. (The expectation value and the strength of the orbital induced magnetic field increases with increasing atomic number. Therefore, the spin−orbit coupling is particularly large for heavy elements.) The Sn atoms with atomic number 50 are much lighter than Pb atoms with atomic number 82; hence, the SOC in tin salts is much weaker than in lead salts.

Varying the size of the QDs, we observe the common confinement effect, that is, an increase of the band gap with decreasing QD size due to the so-called confinement energy, which is defined as the difference between the QD and the corresponding bulk band gap

$$\Delta^{\mathrm{Conf}} = E_g^{\mathrm{QD}} - E_g^{\mathrm{bulk}} \tag{2}$$

It can be modeled using different potential well models. Those depend on the diameter of the nanocrystal D_{NC} and the shape of the confinement potential. In the case of a 3D spherical potential well model (Δ_3^{Conf}), a $1/D_{\mathrm{NC}}^2$ dependence is obtained,[18] while 3D parabolic potential wells (Δ_2^{Conf}) yield a $1/D_{\mathrm{NC}}$ behavior. Sometimes combinations of these two models (Δ_4^{Conf}) are considered.[19] Recent *ab initio* results, however, propose a $D_{\mathrm{NC}}^{-\beta}$ proportionality of the confinement energy (Δ_1^{Conf}) with $\beta < 1$ for small NCs.[20−22] We fit our results using those functional dependencies

$$\Delta_1^{\mathrm{Conf}}[\mathrm{eV}] = \alpha/D_{\mathrm{NC}}^{\beta}[\mathrm{nm}] \tag{3}$$

$$\Delta_2^{\mathrm{Conf}}[\mathrm{eV}] = \alpha/D_{\mathrm{NC}}[\mathrm{nm}] \tag{4}$$

$$\Delta_3^{\mathrm{Conf}}[\mathrm{eV}] = \alpha/D_{\mathrm{NC}}^2[\mathrm{nm}] \tag{5}$$

$$\Delta_4^{\mathrm{Conf}}[\mathrm{eV}] = \alpha/D_{\mathrm{NC}}^1[\mathrm{nm}] + \beta/D_{\mathrm{NC}}^2[\mathrm{nm}] \tag{6}$$

As can be seen in Figure 5 for PbTe QDs (in LDA), the best agreement is achieved for Δ_1^{Conf} with the parameters α, β given in Table 2. This agreement suggests that a theoretical description of QD systems should use 3D spherical potential well models only as a first approximation for QDs with diameters large compared to the bond length. In small QDs with D_{NC} on the order of the cubic lattice constant a_0, the QD−vacuum interface can no longer be modeled as an abrupt transition, but more likely by a continuous potential curve. Therefore, in such cases, the parabolic potential well model yields a better (in the sense of $\beta < 2$) description of the confinement energy as 3D spherical potentials. For the confinement energy model Δ_1^{Conf} and all three compounds, the respective parameters α and β are collected in Table 2. Taking into account SOC effects, the dependence of the band gap on the NC size and the absolute β values are very similar in all three materials.

As we know from Si QDs, the Kohn−Sham (KS) band gap values E_g are already a good approximation for the

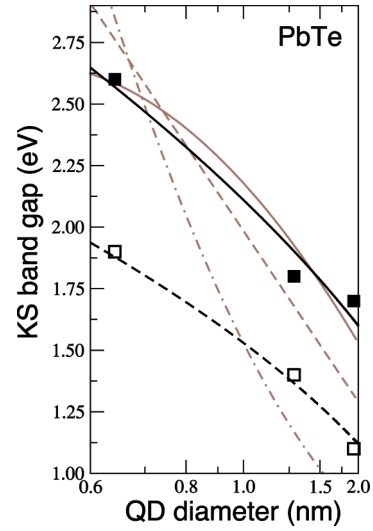

Figure 5. KS band gap of differently sized PbTe QDs with central anion in LDA (filled symbols) and LSDA+SOC (empty symbols). The solid (LDA) or dashed (LSDA+SOC) lines represent the fitted size dependence according to Δ_1^{Conf}. Alternative dependencies Δ_2^{Conf} with $\alpha = 1.4$ (dashed line), Δ_3^{Conf} with $\alpha = 0.92$ (dash-dotted line), and Δ_4^{Conf} with $\alpha = 2.1$ and $\beta = 0.54$ (solid line) in LDA are shown in brown.

electron−hole pair excitation energies E_{pair} due to the almost cancellation of excitonic and quasiparticle effects, which vary as $1/D_{\mathrm{NC}}$.[23] In addition, in larger IV−VI NCs, these many-body effects are small because the bulk electronic dielectric constant ε_∞ is large (ε_∞ = 23−45). Also, other theoretical studies of PbSe QDs assume excitonic effects to be small due to the strong dielectric screening.[24] The calculated excitation energies E_{pair} are given in Table 3. Thereby, E_{pair} is computed as the difference of total energies from two self-consistent calculations (ΔSCF method)[21]

$$E_{\mathrm{pair}} = E_{\mathrm{XS}}(\mathbf{R}_{\mathrm{GS}}) - E_{\mathrm{GS}}(\mathbf{R}_{\mathrm{GS}}) \tag{7}$$

taken at the equilibrium atomic positions $\{\mathbf{R}_{\mathrm{GS}}\}$ of the electronic ground state, while E_{GS} and E_{XS} are the total energies of the NC in the ground and the excited state (with one electron−hole pair), respectively. For the investigated IV−VI semiconductor NCs, we make the same observation as in the case of Si NCs.[23] The KS gaps give a lower limit for the pair excitation energies including both excitonic and electronic relaxation effects.

It is therefore reasonable to compare the KS band gaps as a first estimate with the true HONO−LUNO transition energies whose values are derived from optical absorption experiments. To further justify the D_{NC} variation 3 proposed for the confinement energy Δ_1^{Conf},

TABLE 2. Confinement Energy Parameters α and β According to Δ_1^{Conf} of PbSe, PbTe, and SnTe QDs

	PbSe		PbTe		SnTe	
	α	β	α	β	α	β
LDA	1.9	0.60	1.5	0.61	1.3	0.36
LSDA+SOC	1.4	0.46	1.4	0.53	1.1	0.44

TABLE 3. Calculated KS HONO−LUNO Band Gaps E_g (E_g^*), the Corresponding Electron−Hole Pair Excitation Energies E_{pair} (E_{pair}^*), as well as the Resulting Franck−Condon Shifts ΔE_{FC} and ΔE_{FC}^{gap}[a]

	PbSe			PbTe			SnTe		
D_{NC} (nm)	0.61	1.23	1.84	0.64	1.28	1.92	0.62	1.25	1.87
E_{gap} (eV)	1.91	1.51	1.16	1.93	1.43	1.11	1.74	1.35	1.16
E_{gap}^* (eV)	(1.09)	1.33	1.14	1.79	1.33	1.09	(0.07)	1.21	1.16
E_{pair} (eV)	2.23	1.55	1.17	1.93	1.46	1.13	1.80	1.38	1.16
E_{pair}^* (eV)	(1.47)	1.38	1.17	1.82	1.37	1.11	(0.19)	1.25	1.16
ΔE_{FC} (meV)	(760)	170	>1	110	90	18	(1610)	130	>1
ΔE_{FC}^{gap} (meV)	(827)	185	15	145	96	13	(1670)	133	>1

[a] All listed results are computed with inclusion of SOC and for the ground-state and excited-state (with star) geometries. The gap values are in eV, while the FC shifts are given in meV. The values in brackets for PbSe and SnTe QDs are influenced by H−H* bonds occurring in the excited-state geometry.

we compare our predictions with recent experimental and theoretical band gap values for PbSe QDs in Figure 6. It is obvious that the fit of our data using Δ_1^{Conf} models (expression 3) the measured gap values quite well. Taking into account that the parameters α and β are determined with only three different data points, we find this good agreement remarkable.

The gaps obtained for the ground-state geometry should be observable in optical absorption measurements because optical transitions are much faster than the lattice relaxation. However, in luminescence or fluorescence experiments, the lattice has time to rearrange in the presence of excited electron−hole pairs. The emission peak of semiconductor NCs should therefore usually be red-shifted with respect to the HONO−LUNO absorption peak. This shift is usually extracted from a comparison of optical absorption and emission spectra and identified as Stokes shift. Different contributions to the Stokes shift in NCs have been discussed in the literature: size distribution effects,[30] electron−hole interactions,[27] or the Franck−Condon shift ΔE_{FC}.[12] The latter one was shown to play an important role in small NCs.[12,23,31−34] Within the total energy framework, it can be calculated by pair excitation energies of different geometries

$$\Delta E_{FC} = E_{pair} - E_{pair}^* \quad (8)$$

where

$$E_{pair}^* = E_{XS}(\mathbf{R}_{XS}) - E_{GS}(\mathbf{R}_{XS}) \quad (9)$$

denotes the electron−hole pair excitation energy within the excited-state geometry $\{\mathbf{R}_{XS}\}$. We describe the excited state by the presence of one electron−hole pair, which is modeled *via* an occupation-number constraint. Alternatively, using the above observed similarity, the Franck−Condon shift can also be determined by the difference of the HONO−LUNO band gaps E_g and E_g^* in ground-state and excited-state geometries, respectively:

$$\Delta E_{FC}^{gap} = E_g - E_g^* \quad (10)$$

Results for both types of Franck−Condon shifts are listed in Table 3. The values in brackets for the smallest PbSe and SnTe QDs are influenced by a H−H* bond occurring in the excited-state geometry of these systems; that means, at the QD surfaces, unpassivated dangling bonds may occur. Therefore, these values have to be taken with caution. For QDs with diameters $D_{NC} > 2$ nm, the Franck−Condon shift seems to become negligible. The two types of shifts are similar, but with the general tend $\Delta E_{FC}^{gap} \gtrsim \Delta E_{FC}$. Our results are in good agreement with other theoretical predictions for PbSe QDs.[12] The remaining small differences are attributed to the different passivation schemes.

Optical Properties. The electronic properties have clear consequences for the optical properties. For their demonstration, we have plotted the absorbance, or more precisely, the imaginary part of the dielectric function, Im[$\varepsilon(\omega)$], for PbSe, PbTe, and SnTe QDs of different sizes in Figure 7. As expected from the DOS in Figure 4, in all three cases, Im[$\varepsilon(\omega)$] shows a similar line shape and size variation. As a consequence of the confinement effect, we obtain a red shift and a smoothing of the optical spectra with increasing QD size. Cer-

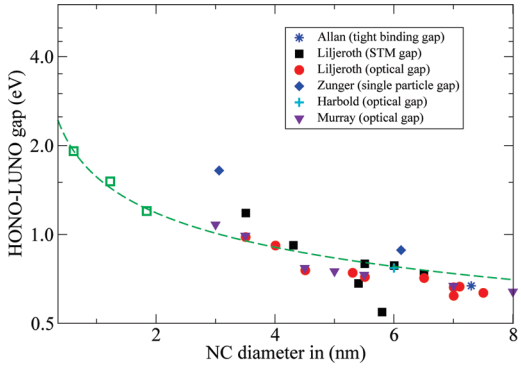

Figure 6. HONO−LUNO gap of PbSe nanodots as computed (green empty squares) or extrapolated with eq 3 (green dashed line). Corresponding experimental and theoretical values are taken from Allan *et al.*,[25] Liljeroth *et al.*,[26] Zunger *et al.*,[27] Harbold *et al.*,[28] and Murray *et al.*[29]

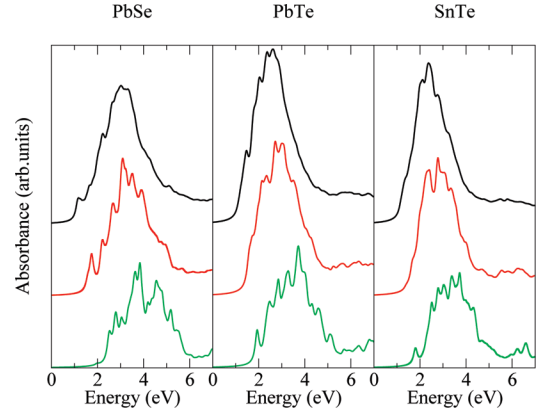

Figure 7. Imaginary part of the dielectric function (absorbance) of PbSe, PbTe, and SnTe QDs of different sizes: QD-1a (green), QD-2a (red), and QD-3a (black).

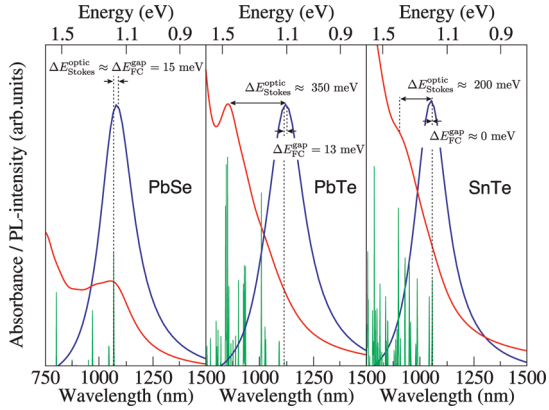

Figure 8. Absorbance (red) and PL (blue) spectra for PbSe, PbTe, and SnTe QD-3a. The energies and oscillator strengths of the optical transitions in the absorbance spectra are marked by vertical green lines. The resulting optical Stokes shift and the Franck−Condon shift are indicated.

tainly, at the onset of the spectra, one observes considerable differences.

In order to understand the different spectral behavior of light absorption and emission, we compare the absorbance and photoluminescence (PL) spectra of the larger 3a-QDs for the three compounds in Figure 8. In the PbTe and SnTe NCs, the HONO−LUNO transition has a relative small oscillator strength compared to other transitions close by. Hence, the first peaks or shoulders in the optical absorbance spectra occur at higher energies than E_g. They are built out of several optical transitions and not only from the lowest-energy one. This results in optical Stokes shifts $\Delta E^{optic}_{Stokes}$ observed from the computed spectra in Figure 8 much larger than the calculated Franck−Condon shifts ΔE^{gap}_{FC}. On the other hand, in the PbSe QD-3a, the HONO−LUNO transition has the largest oscillator strength in the onset region of the absorbance spectra. This leads to a first peak close to the band gap value. Hence, the optical Stokes shift and the Franck−Condon shift are almost equal $\Delta E^{optic}_{Stokes} \approx \Delta E^{gap}_{FC}$. These findings demonstrate that the Franck−Condon shift is generally not able to describe the observed optical Stokes shift. Only in some systems, such as small colloidal PbSe or Si[31−34] QDs, where the HONO−LUNO oscillator strength is relatively large, the Franck−Condon shift represents the main contribution to the optical Stokes shift. In other systems, such as the investigated colloidal PbTe or SnTe QDs, where the HONO−LUNO transition contributes barely to the absorbance spectra, the Stokes shift is much larger than the Franck−Condon shift.

Experimental results concerning colloidal IV−VI semiconductor QDs show a relatively wide range for the optical onset energies as well as for the Stokes shifts. For example, Lifshitz *et al.*[30] measured the Stokes shift of PbSe NCs and PbSe/PbSe$_x$S$_{1-x}$ core/shell NCs as a function of size, shell thickness, and shell composition. They reported Stokes shifts ranging from 100 meV for 4 nm PbSe QDs to −10 meV (anti-Stokes) for 6.1 nm PbSe QDs. On the other hand, under ambient pressure, Zhuravlev *et al.* found a Stokes shift of about 20 meV for 3 nm PbSe QDs.[35] Our result of $\Delta E^{optic}_{Stokes} = 15$ meV for 1.9 nm PbSe QDs fits quite well to the latter result. For colloidal PbTe QDs with 2.9 nm diameter, a Stokes shift of 65 meV was obtained by Murphy *et al.*[36] In fact, our prediction of 350 meV for 1.9 nm PbTe QDs overestimates this value by a factor of 5. This difference may be attributed to different surface passivations and QD shapes. Such differences will, of course, have a strong influence on the electronic states inside the gap region and will, hence, influence the obtained values for the Stokes and Franck−Condon shifts considerably. In the case of colloidal SnTe QDs, up to now, no Stokes shift could be determined experimentally because the absorbance shows no peak structure near the optical onset energy (*i.e.*, in the range of 600−1500 nm), which compares quite well with our prediction (see Figure 8; see supporting material of ref 7).

SUMMARY

We have investigated the structural, electronic, and optical properties of IV−VI semiconductor nanocrystals using *ab initio* methods. In particular, pseudohydrogen passivated colloidal PbSe, PbTe, and SnTe QDs have been used as model systems. Besides an almost unperturbed rocksalt structure, we found a $1/D^{\beta}$ dependence of the confinement energy on the QD diameter with $\beta \sim 0.5$. Therefore, 3D spherical potential well models, which are commonly used in the literature, are not suitable for a precise description of the confinement energy of small QD systems. The calculated electron−hole pair excitation energies are almost equivalent to the KS band gap values, which confirms the small influence of excitonic effects in IV−VI materials.

In addition we have *ab initio* calculated the optical absorbance and to our knowledge, for the first time, the PL signal of the considered IV−VI QDs. Different contributions to the obtained Stokes shift have been discussed. In particular, we could show that the Franck−Condon shift is generally not able to describe the complete optically observed Stokes shift. Rather, one has to take into account all optical oscillators with their strength and energetic position to simulate the absorbance peaks correctly.

METHODS

Theoretical Methods: We apply the density functional theory (DFT) within local-density approximation (LDA) or local-spin density approximation (LSDA) as implemented in the Vienna *ab initio* simulation package (VASP).[37,38] The electronic structure is obtained as eigenvalues and eigenfunctions of the Kohn−Sham (KS) equation. To evaluate the influence of nonscalar relativistic effects, in particular, spin−orbit coupling (SOC), we perform cal-

culations including noncollinear spins.[39] In the case of the heavy elements forming PbTe, SnTe, and PbSe, those effects play an important role. Spin−orbit splittings of the p-like valence electrons are in the range of 1 eV. Since the influence of nonscalar relativistic effects (in particular, spin−orbit coupling) on the structural data is negligible,[40] we do not take those effects into account for the geometry optimization. The interaction of the valence electrons with the remaining ions is modeled by pseudopotentials generated within the projector augmented wave (PAW) method.[41] In IV−VI semiconductors, the outermost occupied d states give rise to shallow semicore bands, which contribute essentially to the chemical bonding.[42] Therefore, we treat the Sn4d and Pb5d electrons as valence electrons. An energy cutoff of 15 Ry for the plane-wave basis is sufficient to obtain converged structural properties. The total-energy expression contains a Brillouin zone (BZ) integration, which is replaced by a summation over special points of the Monkhorst−Pack (MP) type.[43] However, the large size of the supercells justifies the restriction of the **k**-point sampling in the BZ to the Γ point.

Optical Properties: To describe the optical properties of the considered NC systems, we have calculated the dielectric tensor ε_{ij} within the independent-particle approximation. In this approach, the ε_{ij} can be obtained from the eigenfunctions $|n\mathbf{k}\rangle$ and eigenvalues $\varepsilon_n(\mathbf{k})$ of the corresponding Kohn−Sham Hamiltonian, using the Ehrenreich−Cohen formula[44]

$$\varepsilon_{ij}(\omega) = \delta_{ij} + \frac{16\pi e^2\hbar^2}{\Omega}\sum_{\mathbf{k},c,v}\frac{(f_v(\mathbf{k}) - f_c(\mathbf{k}))\langle c\mathbf{k}|v_i|v\mathbf{k}\rangle\langle v\mathbf{k}|v_j|c\mathbf{k}\rangle}{[\varepsilon_c(\mathbf{k}) - \varepsilon_v(\mathbf{k})]([\varepsilon_c(\mathbf{k}) - \varepsilon_v(\mathbf{k})]^2 - \hbar^2\tilde{\omega}^2)} \quad (11)$$

where $\tilde{\omega} = \omega + i\eta$ is the photon frequency provided with a small imaginary part η describing finite lifetime effects and Ω the supercell volume. The matrix elements $\langle c\mathbf{k}|v_i|v\mathbf{k}\rangle$ of the velocity operator v_i with filled valence (v) and empty conduction (c) states are evaluated by calculating the corresponding eigenfunctions. They are correctly described because the PAW method yields all-electron wave functions for the valence electrons.[45] In the ground state, the Fermi functions $f_n(\mathbf{k}) = f(\varepsilon_n(\mathbf{k}))$ of the valence and conduction states are given simply by 1 and 0, respectively. Since the considered NCs are almost central symmetric, the dielectric tensor becomes isotropic $\varepsilon(\omega) = \varepsilon_{xx}(\omega) = \varepsilon_{yy}(\omega) = \varepsilon_{zz}(\omega)$. The imaginary part of the remaining dielectric function is the central quantity describing the optical absorption spectra

$$\alpha(\omega) \sim \mathrm{Im}[\varepsilon(\omega)] \quad (12)$$

The corresponding photoluminescence (PL) spectra can then be formally obtained from expressions 11 and 12 by a replacement of the occupation number factor as[46]

$$I_{PL}(\omega) = \frac{f_c(1 - f_v)}{f_v - f_c}\alpha^*(\omega) \quad (13)$$

where now the Fermi functions f_c and f_v describe the electron and hole distributions after excitation and $\alpha^*(\omega)$ is the optical absorption coefficient in the excited-state geometry.

Nanocrystal Construction and Optimization. To construct IV−VI NCs, we start with an atom in the center of the NC. Then the next atoms are placed shellwise according to the rocksalt structure of these materials. Finally, we cut off the outermost corners and edges to obtain a rhombo-cuboctahedron shape. This method yields NCs with a remaining O_h symmetry and nonstoichiometric anion−cation ratios. Since we are not interested in surface-related effects, we passivate all dangling bond with pseudohydrogen atoms H and H*. The valences (1/3 and 5/3) for an optimal passivation are obtained following an idea of Huang *et al.*[47] The atomic positions are optimized until the Hellmann−Feynman forces are smaller than 20 meV/Å.

Acknowledgment. We acknowledge financial support by the Fonds zur Förderung der Wissenschaftlichen Forschung (Austria) in the framework of SFB25, Nanostrukturen für Infrarot-Photonik (IR-ON), and the EU *via* the I3 project ETSF (GA No. 211956). Grants of computer time from the Höchstleistungsrechenzentrum Stuttgart and Munich are gratefully acknowledged.

REFERENCES AND NOTES

1. Schaller, R. D.; Klimov, V. I. High Efficiency Carrier Multiplication in PbSe Nanocrystals: Implications for Solar Energy Conversion. *Phys. Rev. Lett.* **2004**, *92*, 186601.
2. Ellingson, R. J.; Beard, M. C.; Johnson, J. C.; Yu, P.; Micic, O. I.; Nozik, A. J.; Shabaev, A.; Efros, A. L. Highly Efficient Multiple Exciton Generation in Colloidal PbSe and PbS Quantum Dots. *Nano Lett.* **2005**, *5*, 865.
3. Schaller, R. D.; Agranovich, V. M.; Klimov, V. I. High-Efficiency Carrier Multiplication through Direct Photogeneration of Multi-excitons *via* Virtual Single-Exciton States. *Nature* **2005**, *1*, 189.
4. de Lamaestre, R. E.; Bernas, H.; Pacifici, D.; Franzo, G.; Priolo, F. Evidence for a "Dark Exciton" State of PbS Nanocrystals in Silicate Glass. *Appl. Phys. Lett.* **2006**, *88*, 181115.
5. Kovalenko, M. V.; Talapin, D. V.; Loi, M. A.; Cordella, F.; Hesser, G.; Bodnarchuk, M. I.; Heiss, W. Quasi-Seeded Growth of Ligand-Tailored PbSe Nanocrystals through Cation-Exchange-Mediated Nucleation. *Angew. Chem., Int. Ed.* **2008**, *47*, 3029.
6. Urban, J. J.; Talapin, D. V.; Shevchenko, E. V.; Kagan1, C. R.; Murray, C. B. Synergism in Binary Nanocrystal Superlattices Leads to Enhanced p-Type Conductivity in Self-Assembled PbTe/Ag_2Te Thin Films. *Nat. Mater.* **2007**, *6*, 115.
7. Kovalenko, M. V.; Heiss, W.; Shevchenko, E. V.; Lee, J.-S.; Schwinghammer, H.; Alivisatos, A. P.; Talapin, D. V. SnTe Nanocrystals: A New Example of Narrow-Gap Semiconductor Quantum Dots. *J. Am. Chem. Soc.* **2007**, *129*, 11354.
8. Leitsmann, R.; Bechstedt, F. Electronic-Structure Calculations for Polar Lattice-Structure-Mismatched Interfaces: PbTe/CdTe(100). *Phys. Rev. B* **2007**, *76*, 125315.
9. Albanesi, E. A.; Okoye, C. M. I.; Rodriguez, C. O.; y Blanca, E. L. P.; Petukhov, A. G. Electronic Structure, Structural Properties and Dielectric Functions of IV−VI Semiconductors PbSe and PbTe. *Phys. Rev. B* **2000**, *61*, 16589.
10. Wei, S.-H.; Zunger, A. Electronic and Structural Anomalies in Lead Chalcogenides. *Phys. Rev. B* **1997**, *55*, 13605.
11. Leitsmann, R.; Bechstedt, F. *High Performance Computing in Science and Engineering '07*; Springer: Berlin, Heidelberg, 2008.
12. Franceschetti, A. Structural and Electronic Properties of PbSe Nanocrystals from First Principles. *Phys. Rev. B* **2008**, *78*, 075418.
13. Phillips, J. C. *Bonds and Bands in Semiconductors*; Academic Press: New York, 1973.
14. Schiferl, D. Bonding and Crystal Structures of Average-Valence- <5> Compounds: A Spectroscopic Approach. *Phys. Rev. B* **1974**, *10*, 3316.
15. Kovalenko, M. V.; Kaufmann, E.; Pachinger, D.; Roither, J.; Huber, M.; Stangl, J.; Hesser, G.; Schäffler, F.; Heiss, W. Colloidal HgTe Nanocrystals with Widely Tunable Narrow Band Gap Energies: From Telecommunications to Molecular Vibrations. *J. Am. Chem. Soc.* **2006**, *1281*, 3516.
16. Perebeinos, V.; Chang, S. W.; Zhang, F. Madelung Model Prediction for Dependence of Lattice Parameter on Nanocrystal Size. *Solid State Commun.* **2002**, *123*, 295.
17. Hummer, K.; Grüneis, A.; Kresse, G. Structural and Electronic Properties of Lead Chalcogenides from First Principles. *Phys. Rev. B* **2007**, *75*, 195211.
18. Scherz, U. *Quantenmechanik*; Teubner: Stuttgart, Leipzig, 1999.
19. Cademartiri, L.; Montanari, E.; Calestani, G.; Migliori, A.; Guagliardi, A.; Ozin, G. A. Size-Dependent Extinction Coefficients of PbS Quantum Dots. *J. Am. Chem. Soc.* **2006**, *128*, 10337.
20. Heitmann, J.; Müller, F.; Yi, L.; Zacharias, M.; Kovalev, D.; Eichhorn, F. Excitons in Si Nanocrystals: Confinement and Migration Effects. *Phys. Rev. B* **2004**, *69*, 195309.

21. Weissker, H.-C.; Furthmüller, J.; Bechstedt, F. Optical Properties of Ge and Si Nanocrystallites from *Ab Initio* Calculations. II. Hydrogenated Nanocrystallites. *Phys. Rev. B* **2002**, *65*, 155328.
22. Ramos, L. E.; Furthmüller, J.; Bechstedt, F. Effect of Backbond Oxidation on Silicon Nanocrystallites. *Phys. Rev. B* **2004**, *70*, 033311.
23. Ramos, L. E.; Weissker, H.-C.; Furthmüller, J.; Bechstedt, F. Optical Properties of Si and Ge Nanocrystals: Parameter-Free Calculations. *Phys. Status Solidi B* **2005**, *15*, 3053.
24. An, J. M.; Dudiy, S. V.; Franceschetti, A.; Zunger, A. The Peculiar Electronic Structure of PbSe Quantum Dots. *Nano Lett.* **2006**, *6*, 2728.
25. Allan, G.; Delerue, C. Confinement Effects in PbSe Quantum Wells and Nanocrystals. *Phys. Rev. B* **2004**, *70*, 245321.
26. Liljeroth, P.; van Emmichoven, P. A. Z.; Hickey, S. G.; Weller, H.; Grandidier, B.; Allan, G.; Vanmaekelbergh, D. Density of States Measured by Scanning-Tunneling Spectroscopy Sheds New Light on the Optical Transitions in PbSe Nanocrystals. *Phys. Rev. Lett.* **2005**, *95*, 086801.
27. An, J. M.; Franceschetti, A.; Zunger, A. The Excitonic Exchange Splitting and Radiative Lifetime in PbSe Quantum Dots. *Nano Lett.* **2007**, *7*, 2129.
28. Harbold, J. M.; Du, H.; Krauss, T. D.; Cho, K.-S.; Murray, C. B.; Wise, F. W. Time-Resolved Intraband Relaxation of Strongly Confined Electrons and Holes in Colloidal PbSe Nanocrystals. *Phys. Rev. B* **2005**, *72*, 195312.
29. Murray, C. B.; Sun, S.; Gaschler, W.; Doyle, H.; Betley, T. A.; Kagan, C. R. Colloidal Synthesis of Nanocrystals and Nanocrystal Superlattices. *IBM J. Res. Dev.* **2001**, *45*, 47.
30. Lifshitz, E.; Brumer, M.; Kigel, A.; Sashchiuk, A.; Bashouti, M.; Sirota, M.; Galun, E.; Burshtein, Z.; LeQuang, A.; Ledoux-Rak, I.; Zyss, J. Stable PbSe/PbS and PbSe/PbSe$_x$S$_{1-x}$ Core−Shell Nanocrystal Quantum Dots and Their Applications. *J. Phys. Chem. B* **2006**, *110*, 25356.
31. Franceschetti, A.; Pantelides, S. T. Excited-State Relaxations and Franck−Condon Shift in Si Quantum Dots. *Phys. Rev. B* **2003**, *68*, 033313.
32. Puzder, A.; Williamson, A. J.; Grossman, J. C.; Galli, G. Computational Studies of the Optical Emission of Silicon Nanocrystals. *J. Am. Chem. Soc.* **2003**, *125*, 2786.
33. Degoli, E.; Cantele, G.; Luppi, E.; Magri, R.; Ninno, D.; Bisi, O.; Ossicini, S. *Ab Initio* Structural and Electronic Properties of Hydrogenated Silicon Nanoclusters in the Ground and Excited State. *Phys. Rev. B* **2004**, *69*, 155411.
34. Iori, F.; Degoli, E.; Magri, R.; Marri, I.; Cantele, G.; Ninno, D.; Trani, F.; Pulci, O.; Ossicini, S. Engineering Silicon Nanocrystals: Theoretical Study of the Effect of Codoping with Boron and Phosphorus. *Phys. Rev. B* **2007**, *76*, 085302.
35. Zhuravlev, K. K.; Pietryga, J. M.; Sander, R. K.; Schaller, R. D. Optical Properties of PbSe Nanocrystal Quantum Dots under Pressure. *Appl. Phys. Lett.* **2007**, *90*, 043110.
36. Murphy, J. E.; Beard, M. C.; Norman, A. G.; Ahrenkiel, S. P.; Johnson, J. C.; Yu, P.; Micic, O. I.; Ellingson, R. J.; Nozik, A. J. PbTe Colloidal Nanocrystals: Synthesis, Characterization, and Multiple Exciton Generation. *J. Am. Chem. Soc.* **2006**, *128*, 3241.
37. Kresse, G.; Furthmüller, J. Efficiency of *Ab-Initio* Total Energy Calculations for Metals and Semiconductors Using a Plane-Wave Basis Set. *Comput. Mater. Sci.* **1996**, *6*, 15.
38. Kresse, G.; Furthmüller, J. Efficient Iterative Schemes for *Ab Initio* Total-Energy Calculations Using a Plane-Wave Basis Set. *Phys. Rev. B* **1996**, *54*, 11169.
39. Hobbs, D.; Kresse, G.; Hafner, J. Fully Unconstrained Noncollinear Magnetism within the Projector Augmented-Wave Method. *Phys. Rev. B* **2000**, *62*, 11556.
40. Leitsmann, R.; Ramos, L. E.; Bechstedt, F. Structural Properties of PbTe/CdTe Interfaces from First Principles. *Phys. Rev. B* **2006**, *74*, 085309.
41. Kresse, G.; Joubert, D. From Ultrasoft Pseudopotentials to the Projector Augmented-Wave Method. *Phys. Rev. B* **1998**, *59*, 1758.
42. Wei, S.-H.; Zunger, A. Role of Metal d States in II−VI Semiconductors. *Phys. Rev. B* **1988**, *37*, 8958.
43. Monkhorst, H. J.; Pack, J. D. Special Points for Brillouin-Zone Integrations. *Phys. Rev. B* **1976**, *13*, 5188.
44. Leitsmann, R.; Schmidt, W.; Hahn, P. H.; Bechstedt, F. Second-Harmonic Polarizability Including Electron-Hole Attraction from Band-Structure Theory. *Phys. Rev. B* **2005**, *71*, 195209.
45. Adolph, B.; Furthmüller, J.; Bechstedt, F. Optical Properties of Semiconductors Using Projector-Augmented Waves. *Phys. Rev. B* **2001**, *63*, 125108.
46. Hannewald, K.; Glutsch, S.; Bechstedt, F. Theory of Photoluminescence in Semiconductors. *Phys. Rev. B* **2000**, *62*, 4519.
47. Huang, X.; Lindgren, E.; Chelikowsky, J. R. Surface Passivation Method for Semiconductor Nanostructures. *Phys. Rev. B* **2005**, *71*, 165328.